Applied Catalysis B: Environmental 166–167 (2015) 551–559

Contents lists available at ScienceDirect

Applied Catalysis B: Environmental

journal homepage: www.elsevier.com/locate/apcatb

Construction of $Cu/ZrO_2/Al_2O_3$ composites for ethanol synthesis: Synergies of ternary sites for cascade reaction

Yifeng Zhu[a,b], Xiao Kong[a,b], Shanhui Zhu[a], Fang Dong[a,b], Hongyan Zheng[c], Yulei Zhu[a,c,*], Yong-Wang Li[a,c]

[a] State Key Laboratory of Coal Conversion, Institute of Coal Chemistry, Chinese Academy of Sciences, Taiyuan 030001, PR China
[b] University of Chinese Academy of Sciences, Beijing 100039, PR China
[c] Synfuels China Co., Ltd., Beijing 101407, PR China

ARTICLE INFO

Article history:
Received 24 October 2014
Received in revised form 8 December 2014
Accepted 10 December 2014
Available online 12 December 2014

Keywords:
Hydrogenation
Hydrogenolysis
Ethanol
Cu catalyst
Synergistic effects

ABSTRACT

The hydrogenation of dimethyl oxalate (DMO) to ethanol involves the stepwise hydrogenation of C=O bonds and hydrogenolysis of C—O bonds. In the present work, the assembly of ternary active sites (Cu, ZrO_2, Al_2O_3 sites) for this reaction was investigated. The calcination temperature was demonstrated to have profound influences on the catalytic performance, evolutions of texture and structure properties and functionality of active phases of the ternary catalysts with similar compositions. The $Cu/ZrO_2/Al_2O_3$ catalyst calcined at a high temperature of 750 °C exhibited an ethanol yield up to 97.4% and stable performance (>200 h). Key to success is the concurrence of the stable metallic Cu sites with more proportions of Cu^+ sites, active crystalline ZrO_2 phases and sufficient acid sites which were generated upon high temperature calcination. The high-temperature calcination annealed Cu particles into large ones, facilitating the high stability. Another factor for the good stability is the formation of $CuAl_2O_4$ spinel and the resulted strong interactions between Cu and Al_2O_3 after reduction. Overall, the design of efficient multifunctional catalysts for hydrogenation/hydrogenolysis of C=O/C—O bonds lies in the adequate assembly and modulation of textural, structural and surface properties of catalysts. The structure-performance relationships were well elucidated by the analysis of structural and surface properties of active phases and catalytic performance, which provide more rational choices for making high-performance catalysts for C=O hydrogenation and C—O hydrogenolysis reactions.

1. Introduction

Ethanol, as an alternative fuel, has received much attention because of its great importance for environmental protection and long-term economical advantages [1–3]. The primary synthetic approach of ethanol is the fermentation of starch-containing agricultural feedstocks, which is inherently linked to the food supply [4]. Ethanol synthesis from inedible cellulosic materials without impact on the global food supply is potential, but still needs considerable efforts before industrialization [3]. Aiming at this situation, syngas-to-ethanol technology emerged as a promising alternative route, because syngas can be obtained from versatile materials including fossil fuels, biomass and organic wastes [5,6].

Ethanol can be obtained directly and indirectly from syngas [3,7]. Regardless of the usage of noble metal (e.g., Rh), the direct route also suffered from the low ethanol yield (~30% selectivity at low conversions) due to the methanation and C–C coupling [7,8]. The low ethanol yield caused the problems of product separation and subsequent high operational expenses. A breakthrough for syngas-to-ethanol technology is the indirect route catalyzed by cheaper metals (e.g., Pd, Cu) with higher overall ethanol yield [3,9]. The process contains two steps including CO oxidative coupling to dimethyl oxalate (DMO) (>97% DMO selectivity) and subsequent hydrogenation/hydrogenolysis to ethanol (~85% ethanol selectivity) [3,10]. The first part has been commercialized [9] while the second part has two main technological impediments hindering the industrialization progresses of this technology. One is still insufficient ethanol selectivity, another impediment is the poor stability mainly caused by Cu sintering at high reaction temperatures [11].

DMO hydrogenation to ethanol is a cascade reaction containing the stepwise hydrogenation of ester groups to ethylene glycol and the subsequent hydrogenolysis of C—O bonds to ethanol

* Corresponding author at: State Key Laboratory of Coal Conversion, Institute of Coal Chemistry, Chinese Academy of Sciences, Taiyuan 030001, PR China.
Tel.: +86 351 7117097; fax: +86 351 7560668.
E-mail address: zhuyulei@sxicc.ac.cn (Y. Zhu).

http://dx.doi.org/10.1016/j.apcatb.2014.12.015
0926-3373/

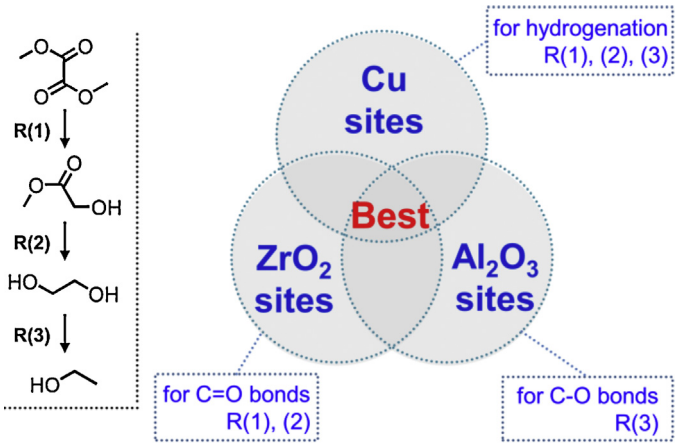

Scheme 1. Assembly of synergistic ternary (Cu, ZrO_2, Al_2O_3) sites for hydrogenation of DMO to ethanol.

($C_4H_6O_4 + 5H_2 = C_2H_5OH + 2CH_3OH + H_2O$, Scheme 1). Supported Cu catalysts have been intensively used and screened as the best catalytic systems for their excellent ability in hydrogenation/hydrogenolysis of C=O/C—O bonds [10,12,13]. The C =O/C—O bonds tend to adsorb over Cu^+ sites while H_2 can be dissociated by Cu^0 sites [14]. Along this line, efforts for making a high-performance catalyst have predominantly focused on the dispersion of Cu phases with balanced Cu^0–Cu^+ sites (e.g., copper phyllosilicate catalysts) while the direct contributions of supports were rarely investigated [10,14,15]. The resulted highly dispersed Cu nanoparticles (NPs) over supports could exhibit good activity for ethanol synthesis. However, they would easily aggregate and deactivate at high temperatures, due to the low Hüttig (134 °C, the temperature at which defective atoms will diffuse) and Tamman (405 °C, that at which bulk atoms will be mobile) temperatures of Cu [16]. The difficulties in improving both the ethanol yield and stability lie in an insufficient understanding of active sites which are known to simultaneously catalyze both C=O hydrogenation and C—O hydrogenolysis and are more stable than active Cu sites [6,16–19].

In view of these problems, it would be highly desirable to elucidate and fully utilize the support components, because catalytic support is an indispensable part of catalysts. We here provide other options to promote both the reactivity and stability from the aspects of supports. Crystalline ZrO_2 (tetragonal and monoclinic) can act as co-active site for activation of C=O bonds and has attracted attentions for reactions involving C=O conversions [6,11,16,20]. The crystalline phases can be obtained by annealing the amorphous ZrO_2 precursor. When ZrO_2 composited with Cu, it needs to be motivated into crystalline phases at higher temperatures [16]. It is also conceivable that Cu phases would be simultaneously annealed into stable and large particles. The active crystalline ZrO_2 and stable Cu sites together lead to an improved catalytic efficiency and stability [16]. Acidic Al_2O_3 can directly contribute to the hydrogenolysis of hydroxymethyl groups [6,21] while the calcination temperature plays critical roles on tuning the acidity [22]. The acid sites can facilitate the subsequent hydrogenolysis of C—O bonds when the ester groups of DMO were saturated into hydroxymethyl groups [6,11]. Therefore, it is imperative to construct a composite which includes metallic Cu, ZrO_2 and acidic Al_2O_3 sites (Scheme 1), for efficient synthesis of ethanol via cascade hydrogenation of C=O bonds and hydrogenolysis of C—O bonds. The metallic Cu^0 sites are expected to adsorb/activate H_2, while the oxide components (ZrO_2 and Al_2O_3) could benefit the activation of C=O/C—O bonds. Thus, the reactivity would be not only determined by Cu sites but also promoted by the oxide components. Moreover, these oxides are more stable than Cu sites under the reaction conditions, which would be useful for enhancement of the catalyst stability.

In this work, we assembled three types of active phases (metallic Cu, ZrO_2 and acidic Al_2O_3 sites) to catalyze ethanol synthesis for the first time. The synergies of the ternary components were progressively modulated by annealing the catalysts at elevated temperatures. Specifically, (1) the high-temperature calcination motivated amorphous ZrO_2 into more active crystalline phases, (2) the high-temperature clacination induced proper amount of acid sites over the surface, (3) it also facilitated the strong interactions between CuO and Al_2O_3 and the formation of $CuAl_2O_4$, generating more proportions of Cu^+ sites over the reduced catalysts, (4) the stable large Cu particles, together with the enhanced strong interactions upon high-temperature calcination facilitate the stability of catalysts. The ternary composites thus exhibit superior ethanol yield and catalyst stability for DMO hydrogenation via the assembly of ternary sites and modulation by calcination temperatures. The work here provides more diverse choices for making high-performance catalysts to synthesize ethanol. The structural evolutions, the changes of surface properties and formation of active phases were investigated in detail by various characterizations and correlated to the catalytic performance. The results are expected to add some new dimensions for exploring the assembly and evolutions of ternary sites by modulating calcination temperature. Moreover, the structure-performance relationship could be useful for further catalyst design for C=O hydrogenation and C—O hydrogenolysis reactions.

2. Experimental

2.1. Catalyst preparation

The following materials have been used for the preparation of catalysts: copper(II) nitrate trihydrate, aluminum(III) nitrate nonahydrate, zirconium(IV) nitrate pentahydrate and ammonium bicarbonate. All these chemicals were purchased from Sinopharm. Co., Ltd., and used without further purification. The catalysts were prepared by co-precipitation method as follows. An aqueous solution containing copper(II) nitrate trihydrate, aluminum(III) nitrate nonahydrate and zirconium(IV) nitrate pentahydrate was prepared and the total metal ions were set as 2 mol/L. An aqueous solution of NH_4HCO_3 (1.5 mol/L) was employed as precipitating agent. Then, the precursor solution was introduced dropwise into a 2 L vessel at 70 °C; the pH value was maintained at 5 ± 0.2. The resulted precipitate was washed, filtered and dried at 110 °C, and then calcined in air at a certain temperature for 5 h with a heating rate of 1.5 °C/min. The as-synthesized catalyst was sieved into particles of

20–40 meshes before use. The catalysts were denoted as CZA-*T*, of which *T* means the calcination temperature. The resulted catalysts have the nominal CuO:ZrO_2:Al_2O_3 mass ratio = 2:1:1 which is based on our previous work [16].

2.2. Catalytic tests

The catalytic test was performed over a fix-bed reactor (inner diameter, 12 mm; length, 600 mm) with a feed stock of 15 wt% DMO in 1,4-dioxane and H_2. The system pressure is 4 MPa and H_2/DMO molar ratio is 150. Prior to the test, the catalyst (20–40 mesh) was loaded and in-situ reduced by 5 vol% H_2/N_2 at 250 °C for 2 h. The products were collected into a cold trap (150 mL), and then analyzed using a GC instrument equipped with a FID detector. The conversion and product selectivity were calculated based on the following equations:

$$\text{Conversion}(\%) = 100 - \frac{\text{Amount of feedafter reaction(mol)}}{\text{Total amount of feed(mol)}} \times 100$$

$$\text{Selectivity}(\%) = \frac{\text{Amount of a product(mol)}}{\text{Total amount of feedconverted (mol)}} \times 100$$

2.3. Characterizations

The elemental analysis was tested using an ICP optical emission spectroscopy (Optima2100DV, PerkinElmer).

The BET surface area was determined via N_2 physical adsorption at −196 °C by a Micromeritics ASAP 2420 instrument. Prior to the measurements, the samples were degassed under vacuum at 90 °C for 1 h and 350 °C for 8 h. The experimental error of BET surface area is within ±10%.

XRD patterns were recorded by a X-ray diffractometer (MiniFlex II, Rigaku) with Cu kα radiation operating at 40 kV, with a rate of 4 °C/min.

Raman patterns were recorded with a LabRAM HR800 system equipped with a CCD detector at room temperature. The 325 nm of the He–Cd laser was used as the exciting source with a power of 30 MW. A 60% reduction of laser output was chosen for the samples to ensure that the samples were not damaged. The power of the laser at the sample (~0.4 mW) was measured by an optical power meter (Thorlabs PM 100D) equipped with S120VC photodiode power sensor.

Temperature programmed reduction (TPR) and N_2O titration experiments were conducted on a Tianjin XQ TP-5080 instrument equipped with a TCD detector. For TPR experiments, 20 mg catalyst was loaded into a quartz tube and heated in 30 mL/min of 10 vol% H_2/N_2 at a rate of 10 °C/min. The Cu surface area was determined by N_2O titration experiments based on the equation of $2Cu + N_2O \rightarrow N_2 + Cu_2O$. The catalysts were pre-reduced at 250 °C for 2 h. Then, they were exposed to 1 vol% N_2O/N_2 flow for 1 h at 30 °C to oxidize the surface Cu^0–Cu_2O. Finally, the samples were re-reduced with a TPR program. The Cu specific area was estimated from the consumption with 1.46×10^{19} copper atoms per square meter.

Temperature programmed desorption of NH_3 (NH_3–TPD) experiments were conducted on the AutoChem II. 2920 instrument (Micromeritics, USA) equipped with a mass spectrum detector. Prior to the tests, the catalysts were pretreated in He flow at 350 °C to remove the adsorbed species for 1 h. After cooling to the room temperature, the catalysts were saturated with NH_3 and then purged with He to remove the physisorbed NH_3 at 100 °C for 30 min. Subsequently, the catalysts were heated to 700 °C with a rate of 10 °C/min.

X-ray photoelectron spectroscopy (XPS) was performed on a Thermo XPS ESCALAB 250Xi spectrometer with a monochromatic Al Kα (1486.8 eV) source. The XPS experiments of reduced samples were performed after an in-situ reduction at 250 °C for 2 h. The obtained binding energies were calibrated using the C1s peak (284.6 eV) as the reference. The experimental error is within ±0.1 eV.

3. Results

3.1. Characterizations of catalysts

The physicochemical and surface properties of Cu/ZrO_2/Al_2O_3 catalysts (CZA-*T*; *T* means the calcination temperature) are summarized in Table 1. Rising calcination temperature in the range of 350–650 °C resulted in the gradual loss of BET surface area from 192.6 to 136.8 m^2/g. The further elevation of temperature caused the dramatic decreases in BET surface area, indicating that obvious sintering of catalysts occurred during the calcination at high temperatures. Cu loadings of all the catalysts determined by ICP analysis were close to the nominal value of 40 wt%, while the Al_2O_3/ZrO_2 mass ratios were slightly lower than the nominal ratio of 1. The ICP results revealed that all the CZA-*T* catalysts had similar bulk elemental compositions. However, unlike the ICP results, the surface elemental compositions determined by XPS experiments showed that the surface Cu contents varied in the range of 20–33 wt% and the Al_2O_3/ZrO_2 ratios were greatly higher than the nominal ratio. The combination of ICP and XPS results demonstrated that Al_2O_3 component was enriched over the catalyst surfaces and other components (CuO and ZrO_2) were embedded in bulk phase. The surface Cu contents increased firstly, reached a maximum at calcination temperature of 550 °C, and decreased with further increases in calcination temperature. The trend of surface Al_2O_3/ZrO_2 ratios was similar to that of surface Cu contents. The metallic Cu specific areas (S_{Cu}) were measured by N_2O titration method. They followed a trend similar to the observations of XPS

Table 1
Main physiochemical properties of CZA catalysts.

Catalysts	S_{BET} (m^2/g)[a]	Cu content (wt%)[b]	Al_2O_3/ZrO_2 ratio (g/g)[b]	Surface Cu content (wt%)[c]	Surface Al_2O_3/ZrO_2 ratio (g/g)[c]	S_{Cu} (m^2/g)[d]	d_{CuO} (nm)[e]	CuO/$CuAl_2O_4$ ratio (mol/mol)[f]
CZA-350	193	39.1	0.84	20.2	3.6	15.2	16.7	–
CZA-450	160	39.4	0.83	30.6	5.0	23.0	18.3	–
CZA-550	160	39.6	0.83	32.7	5.3	27.9	18.4	–
CZA-650	137	39.4	0.83	30.3	4.5	24.4	20.0	–
CZA-750	76	39.3	0.84	26.7	4.5	18.4	21.6	9.2
CZA-850	10	39.7	0.80	27.2	4.3	9.5	25.9	1.9

[a] Determined by N_2 adsorption experiments.
[b] Determined by ICP experiments.
[c] Calculated from XPS data of reduced samples.
[d] Determined by N_2O titration measurements.
[e] Calculated by CuO (1 1 1) reflection based on Scherrer equation.
[f] Determined by TPR experiments.

results. Among the catalysts, the CZA-550 composite exhibited the highest S_{Cu}.

The XRD patterns of calcined CZA-*T* catalysts are shown in Fig. 1. Evident diffraction peaks of CuO at 35.6^0 and 38.7^0 (PDF#48-1548) were observed over all the catalysts. The peaks shaped and intensified with the increase in calcination temperature, indicating a progressive crystallite growth of CuO (Table 1). The particle growth of CuO may cause the loss of metallic Cu specific areas after the catalysts were reduced [23]. As evidenced by N_2O titration and XPS results, the exposed surface Cu sites increased with the calcination temperature in 350–550 °C while decreased when the temperature was further elevated. The XRD results indicated an evident particle growth of CuO in 550–850 °C (Table 1), fitting well with the observations of N_2O titration and XPS analysis. However, the XRD results are seemingly in conflict with the N_2O titration and XPS results in 350–550 °C. The discrepancy can be attributed to the fact that CuO species were partially covered by Al_2O_3 and/or ZrO_2 components [24]. The CuO particles over CZA-350 catalyst were small but partially embedded in the oxide components. Calcination at high temperatures (450 and 550 °C) caused both the enrichment over the surface and sintering of CuO species and comprehensively increased the numbers of surface Cu sites. At higher temperatures (>550 °C), the sintering of CuO particles would dominate over the catalysts, resulting in the decreasing trend of surface metallic Cu concentrations. The evolutions of CuO species over the catalysts, as demonstrated by XRD, N_2O titration and XPS analysis, are in accordance with the previous report on Cu/ZrO_2 catalysts [24].

No diffraction peaks related to Al_2O_3 were observed over all the patterns, indicating the X-ray amorphous state of Al_2O_3. Upon calcination at 750 °C, weak diffraction peaks at 31.3, 36.9 and 44.9^0 emerged, which indicated the formation of $CuAl_2O_4$ spinel (PDF#33-0448) through high-temperature solid-oxide reaction between CuO and Al_2O_3 [25,26]. The peaks of $CuAl_2O_4$ intensified with the further increase of calcination temperature, indicating the particle growth of $CuAl_2O_4$ species.

For ZrO_2 species, the CZA-*T* catalysts calcined at low temperatures (<650 °C) exhibited no observable diffraction peaks related to crystalline ZrO_2, indicating the presence of X-ray amorphous structure and/or existence of very small ZrO_2 crystallites. When the catalyst was calcined at 750 °C, the peaks at 30.3 and 50.4^0 emerged. The peaks can be attributed to the diffractions of tetragonal ZrO_2 (PDF#50-1089). In compared with pure ZrO_2 prepared by similar coprecipitation method, the formation of tetragonal phase was greatly retarded, indicating the strong interactions between CuO and ZrO_2 [16]. Further rising the calcination temperature

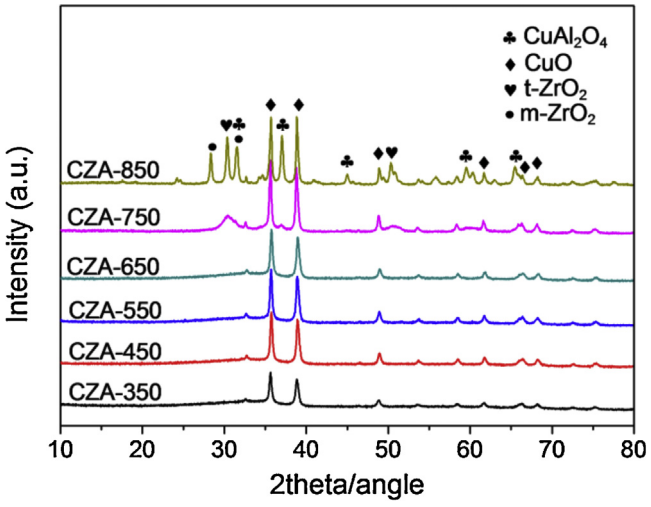

Fig. 1. XRD patterns of CZA-*T* catalysts.

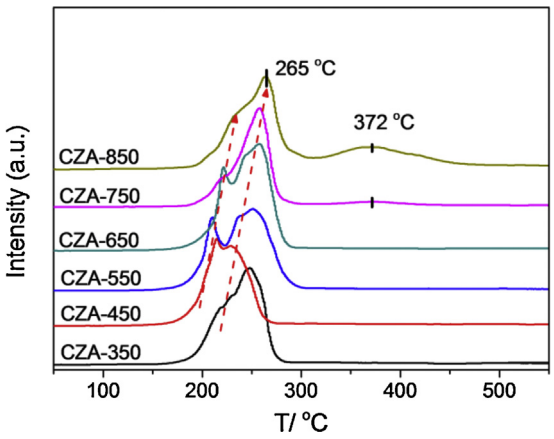

Fig. 2. TPR profiles of CZA-*T* catalysts.

intensified the diffraction peaks and caused the transformation of tetragonal-to-monoclinic, as evidenced by the patterns of monoclinic ZrO_2 at 28.2 and 31.5^0 (partially overlapping with the $CuAl_2O_4$ (220) characteristic) (PDF#37-1484).

To further investigate the reducibility and structural evolutions of catalysts, TPR experiments were performed (Fig. 2). The samples all exhibited a broad reduction peak (150 ~ 300 °C) and a pronounced shoulder at the lower-temperature side, which could be attributed to the reduction of CuO species. The double-peak profiles could be attributed to the stepwise processes of $Cu^{2+} \rightarrow Cu^{+} \rightarrow Cu^0$ [11,19,27]. Interestingly, despite that the CZA-350 had smaller CuO particle size, CZA-350 showed a higher reduction temperature than that of CZA-450 catalyst. As reported earlier by Behrens et al. [28], the crystalline CuO species are easier to be reduced than the highly dispersed CuO embedded under the unreducible oxides, due to the mass-transfer limitation and the strong interactions between CuO and the oxides. The high reduction temperature of CZA-350 indicated that the well-dispersed CuO particles were embedded over the oxides and supported the observations on XPS, N_2O titration and XRD experiments. For the catalysts calcined in the range of 450–850 °C, the reduction profiles of catalysts migrated toward high temperature, indicating the progressive particle growth of CuO over the surface. The CZA-750 and CZA-850 catalysts both exhibited the reduction peaks around 370 °C (see Fig. S1 for details of CZA-750 and CZA-850). According to Huang et al. [29], the reduction of $CuAl_2O_4$ spinel is more difficult than the CuO species. The peaks at 370 °C could be attributed to the reduction of $CuAl_2O_4$ spinel, which is in accordance with the XRD results. The ratios of $CuO/CuAl_2O_4$ were calculated by fitting the TPR data and listed in Table 1. The TPR results confirmed the structural evolutions of CuO species upon rising the calcination temperature: (1) enrichment of CuO over the catalyst surface, (2) progressive particle growth of CuO, (3) formation of $CuAl_2O_4$ spinel through solid reaction between CuO and Al_2O_3 at high temperatures.

Raman results indicated the state changes of CuO species over the catalysts (Fig. 3). Three Raman bands at 293, 345 and 626 cm^{-1} were observed, which could be attributed to the vibrations of the Cu—O and Cu—O—Cu bonds in CuO lattice [30,31]. No obvious Raman feature of other species was detected. The peaks of CZA-350 catalyst exhibited the lowest intensity of CuO characteristics. For the catalysts calcined at 350–650 °C, the bands intensified with the increase of calcination temperature. The results indicated the particle growth of CuO over the catalyst composites and were in good accordance with the XRD experiments [11]. However, further increasing the calcination temperature resulted in the broadening and red-shift of Raman peaks, indicating the change of vibrations of the Cu—O and Cu—O—Cu bonds. Considering that the CuO particle

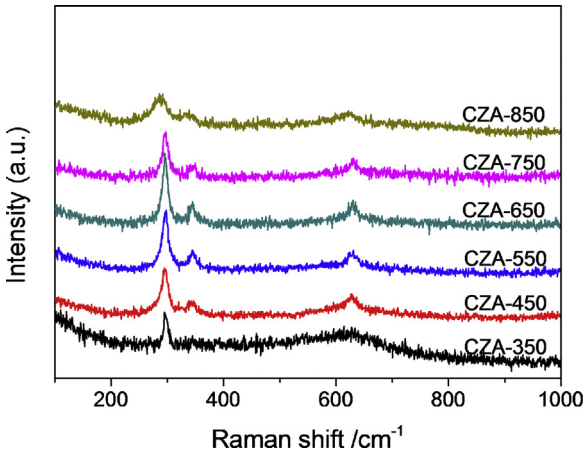

Fig. 3. Raman patterns of CZA-*T* catalysts.

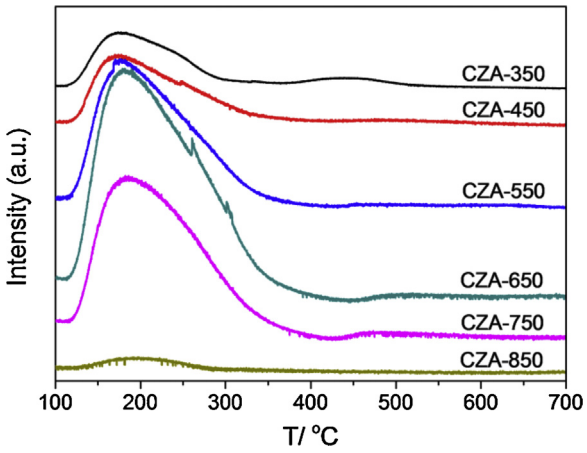

Fig. 4. NH_3–TPD profiles of CZA-*T* catalysts.

sizes were grow and the $CuAl_2O_4$ spinel was formed, the broadening and red-shift of peaks could be attributed to the formation of spinel structure and change of CuO. The Raman results further confirmed the structural evolutions of CuO species.

The acid centers over the surface are believed to influence the efficiency of C—O hydrogenolysis [11,32,33]. Thus, NH_3–TPD experiments were employed to determine the surface acid properties of CZA-*T* catalysts (Fig. 4). With the increase of calcination temperature in 350–650 °C, the density of surface acid sites increased while the strength of acid sites had negligible changes. The increase of surface acidity could be attributed to the dehydration of surface hydroxyl groups [34,35]. The dehydration of hydroxyl groups would induce some freed and defective Al^{3+} ions; and thus, increased the density of surface acid sites [22]. The CZA-650 catalyst had the highest total amount of acid sites among the catalysts. With the further increase of calcination temperature, the amount of surface acid sites decreased gradually. In particular, anneal at 850 °C caused the significant loss of surface acidity. This is because of the sintering of catalyst and the loss of surface area [22,36,37].

XPS experiments were employed to determine the chemical states of Cu, Al and Zr upon calcination and reduction. Fig. 5 shows the Cu 2p XP spectra of calcined and reduced CZA-*T* catalysts and the X-ray excited Auger electron spectroscopy (XAES) spectra of reduced catalysts. The calcined CZA-*T* catalysts all exhibited the Cu $2p_{3/2}$ (~933.6 eV), Cu $2p_{1/2}$ peaks (~953.3 eV) and a serial of satellites, which are the characteristics of Cu^{2+} species over the catalyst surfaces [38]. Upon in-situ reduction at 250 °C, both the Cu $2p_{3/2}$ (~932.8 eV) and Cu $2p_{1/2}$ (952.6 eV) peaks intensified and shifted toward lower binding energy (B.E.), indicating that the Cu^{2+} species were reduced into $Cu^{\delta+}$ species with lower valences (e.g., Cu^0 and Cu^+). For the reduced CZA-850 catalyst, the satellite peaks did not disappear completely, indicating that the Cu^{2+} species were not totally reduced. These unreduced Cu^{2+} species may originate from $CuAl_2O_4$ spinel over the catalyst, as evidenced by TPR results. To further differentiate the Cu^+ species from Cu^0 species, XAES profiles of the reduced catalysts are shown in Fig. 5c. The peak at 918.9 eV was observed for CZA-350 catalyst which is associated with Cu^0 sites [11]. For the CZA-*T* catalysts calcined at higher temperatures, the peaks shifted toward lower kinetic energy values, indicating that the proportion of $Cu^{\delta+}/Cu^0$ increased over the catalyst surfaces [39,40].

The Al 2p peak is located at ~73.9 eV, greatly overlapping with Cu $3p_{3/2}$ (~74.9 eV) and Cu $3p_{1/2}$ (~77.3 eV) peaks [41]. Thus, deconvolutions of peaks in the range of 70–85 eV were performed (Fig. 6). The Al 2p, Cu $3p_{3/2}$ and Cu $3p_{1/2}$ peaks can be easily distinguished. The Al 2p peaks all located around 73.9 eV, with a slight shift toward higher B.E. value (74.1 eV) for CZA-850 catalyst. Ebina et. al. [42] reported that the B.E. values of octahedral and tetrahedral Al sites are 74.5 and 73.7 eV, respectively. According to the B.E. values of Al 2p peaks, the Al cations over the reduced catalysts existed in both octahedral and tetrahedral states. The shift of B.E. value for CZA-850 catalyst indicated that the catalyst contained more octahedral Al cations than other samples. The Al^{3+} cations of $CuAl_2O_4$ spinel mainly exist in 6-coordination (octahedral sites) [43,44]. Thus, the shift of Al 2p over the reduced CZA-850 catalyst indicated the remnant of $CuAl_2O_4$, confirming the existence of unreduced Cu^{2+} sites and convincing the results observed in Cu 2p and XAES profiles.

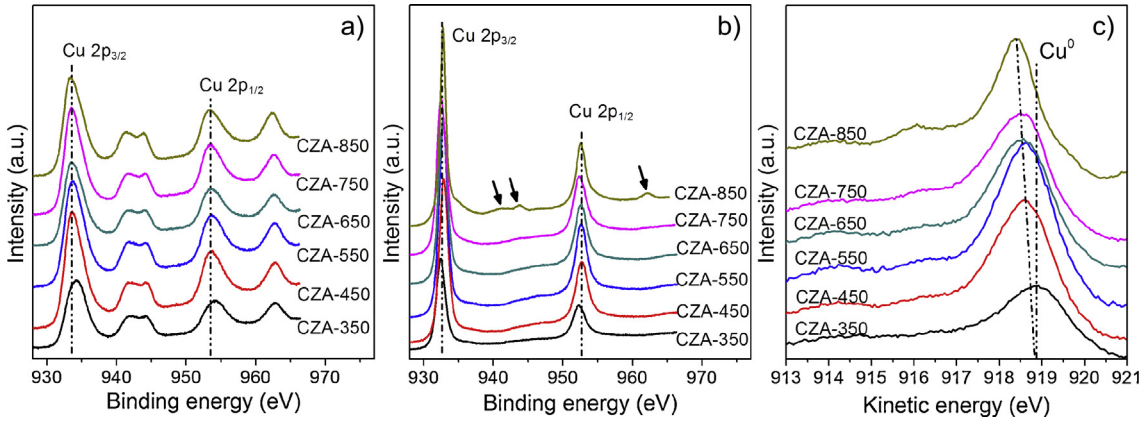

Fig. 5. Cu 2p XP spectra of unreduced (a) and reduced (b) CZA-*T* catalysts, Cu XAES spectra of reduced CZA-*T* catalysts (c).

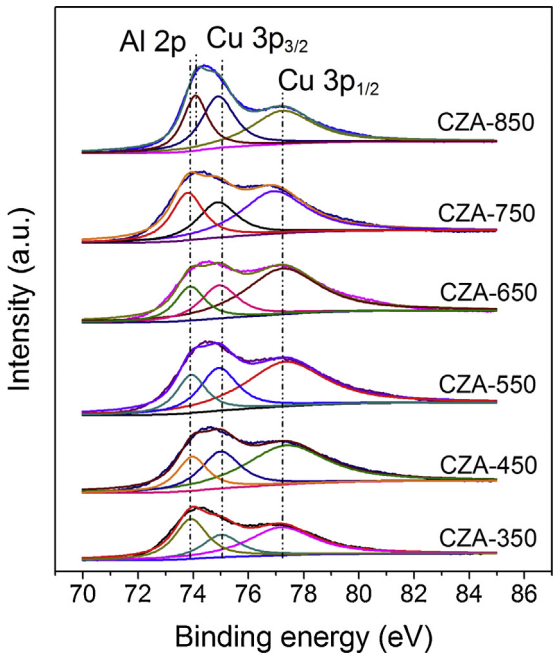

Fig. 6. Al 2p XP spectra of reduced CZA-*T* catalysts.

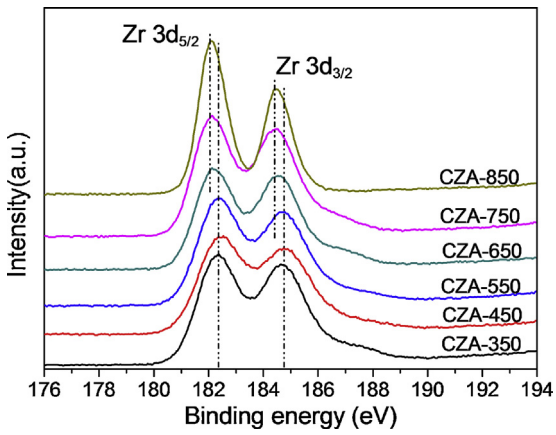

Fig. 7. Zr 3d XP spectra of reduced CZA-*T* catalysts.

Fig. 7 exhibits the Zr 3d spectra of reduced CZA-*T* catalysts. Two peaks in the range of 180–188 eV were observed, which could be attributed to Zr $3d_{5/2}$ and Zr $3d_{3/2}$ peaks. The peaks intensified and sharped with the elevation of calcination temperatures. This is because of the particle growth and enrichment of ZrO_2 species over the surface upon calcination, which is in accordance with the XRD results and elemental analysis of XPS experiments. Moreover, the shifts toward lower B.E. (~0.4 eV) were emerged for the reduced CZA-650, 750 and 850 catalysts. It can be attributed to the formation of Zr species with higher electron density [45]. The slightly reducible Zr species can be generated by doping of Cu^{2+} into ZrO_2, reduction of Cu^{2+} ions and departure of oxygen from the ZrO_2 crystallites, as a result of the strong interactions between Cu and ZrO_2 [6].

3.2. Catalytic performance of $Cu/ZrO_2/Al_2O_3$ ternary catalysts

The catalytic reactivity and stability of CZA-*T* catalysts are shown in Fig. 8. At weight hourly space velocity (WHSV) of 0.3 h^{-1}, the DMO conversions were 100% and the ethanol yields were higher than 78% over all the catalysts (Fig. 8a and Table S1). The ethanol selectivity over CZA-*T* catalysts increased firstly with the elevated calcination temperature in 350–750 °C and decreased when the calcination temperature increased into 850 °C. The main byproduct was 2-methoxyethanol which is formed by the etherification between the generated intermediate ethylene glycol and methanol [11,46]. The selectivity of 2-methoxyethanol showed an adverse tendency with the selectivity of ethanol, indicating the insufficient ability of catalysts for C—O hydrogenolysis [6]. Among these catalysts, the CZA-750 catalyst showed an ethanol yield up to 97.4%, which is the best one reported to our knowledge. It should be noted that high proportions of other products (methyl glycolate and ethylene glycol) were formed over CZA-850 catalysts, indicating the insufficient hydrogenation ability of catalysts and insufficient acid sites for hydrogenolysis. To differentiate the performance of catalysts more remarkably, the tests were also performed at a high WHSV of 0.6 h^{-1} (Fig. 8b and Table S1), of which the results demonstrated similar trends with the tests at 0.3 h^{-1}. The ethanol yield of CZA-750 catalyst only decreased about 8.7% when the WHSV is doubling, implying the high activity and ethanol selectivity of the catalyst. Ethanol synthesis from DMO hydrogenation–hydrogenolysis was always performed at high temperatures (>270 °C) to facilitate the cleavage of C—O bonds. The supported Cu catalysts would easily deactivate due to the growth and sintering of metal particles at such a high reaction temperature [11]. Thus, the stability is another major concern for the develop-

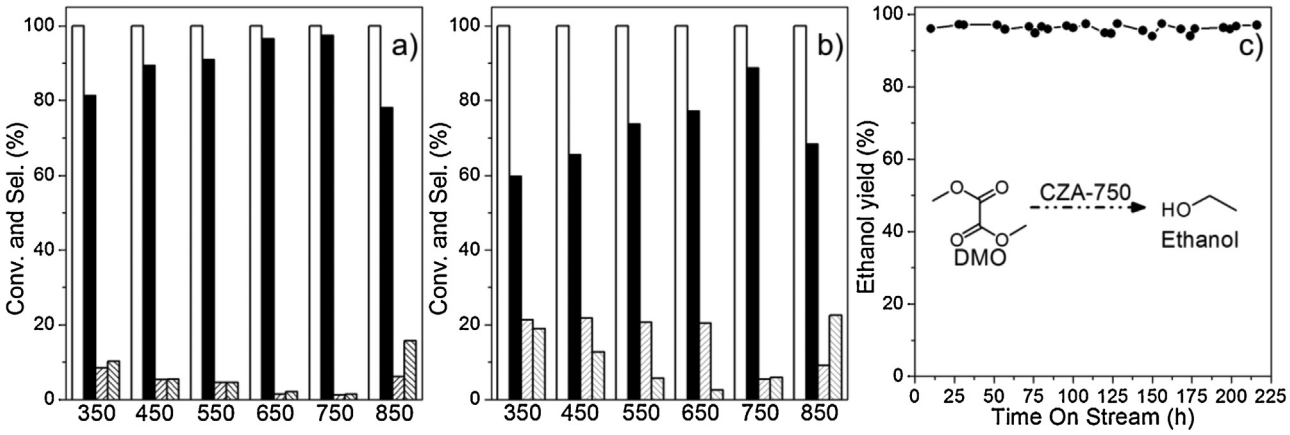

Fig. 8. Conversion and product selectivity (DMO conversion (□), ethanol (■), 2-methoxyethanol (▨), others (▧)) of CZA-*T* catalysts (a) the performance at WHSV = 0.3 h^{-1}. (b) The performance at WHSV = 0.6 h^{-1}. Conditions: 270 °C, 4 MPa, H_2/DMO = 150) and the stability of CZA-750 catalyst, (c) conditions: 270 °C, 4 MPa, H_2/DMO = 150, WHSV = 0.3 h^{-1}).

ment of high-performance catalysts [11,47]. In our previous work, the co-precipitated Cu/Al_2O_3 catalyst calcined at 450 °C only exhibited 80 h lifespan, despite of the high ethanol yield of ~95% [11]. As shown in Fig. 8c, the CZA-750 catalyst exhibited a stable ethanol yield throughout 200 h tests at 270 °C, indicating the high stability of catalyst and the potential for industrial applications.

4. Discussions

4.1. The evolutions of structural and surface properties

The above characterizations visualized the evolutions of microstructures, physicochemical and surface properties of catalysts and the construction of ternary functional components upon calcination and reduction. In particular, these parameters were greatly influenced by the calcination temperature. Scheme 2 summarized the main structural evolutions of the ternary active phases (CuO, ZrO_2 and Al_2O_3) upon increasing the calcination temperature. For CuO species, elevation of calcination temperature induced the growth of CuO particles, surface enrichment of CuO phases and the formation of $CuAl_2O_4$ spinel. When the catalyst was calcined at 350 °C, the CuO particles were highly dispersed but they were partially covered by other oxides. The enrichment of other oxides (e.g., Al_2O_3) over the surface caused a high reduction temperature of CuO and low exposed surface Cu^0 sites. When the temperature was increased, CuO particles became larger but enriched over the surface; and thus, the surface metallic Cu sites increased. The further increase of calcination temperature would decrease the metallic Cu sites because the particle sintering dominated over the catalysts. This phenomenon was also observed over Cu/ZrO_2 catalysts prepared by oxalate gel-coprecipitation technique [24]. The high temperature calcination (750 and 850 °C) also induced the formation of $CuAl_2O_4$ spinel. Among the catalysts, CZA-550 catalyst exhibited the highest surface Cu^0 sites. For ZrO_2 component, it transformed with the sequence of amorphous → tetragonal → monoclinic phases when the calcination temperature was increased from 350 to 850 °C. It should be noted that compared with the pure ZrO_2 prepared by the similar method, the formation and transformation of crystalline ZrO_2 were greatly retarded [16]. This is because of the strong interactions between CuO and ZrO_2 phases by doping of Cu^{2+} into the structure of ZrO_2 [11,16,17].

The chemical states of elements and surface properties were also changed with the variation of structural parameters. Except for the surface Cu^0 concentrations, the reducibility of CuO species and the proportions of surface Cu^+ sites of reduced catalyst were modulated. The $CuAl_2O_4$ spinel was more difficult to be reduced than CuO species [25], as evidenced by the TPR results. Al 2p spectra indicated that slight residual $CuAl_2O_4$ spinel even existed in the reduced CZA-850 catalyst. This led to the formation of more positive Cu species (e.g., Cu^+) over the catalysts calcined at high temperatures, as evidenced by the Cu XAES spectra of reduced catalysts.

The amount of surface acid sites increased continuously in 350–650 °C. According to Peri et al. [34,35], rising the calcination temperature would diminish the surface hydroxyl groups and generate more unsaturated/defective Al^{3+} sites; and thus, motivate more surface acid sites. However, further increase of calcination temperature in 650–850 °C resulted in the loss of surface acidity concentration. This is due to the loss of surface area and sintering of catalyst composites [22,36,37]. CZA-850 catalyst only exhibited slight surface acidity.

As revealed before, the strong interactions between CuO and ZrO_2 phases can facilitate the formation of vacancies by Cu^{2+} doping into crystalline ZrO_2, Cu^{2+} reduction, and departure of oxygen from crystalline ZrO_2 [16]. Thus, the catalysts with crystalline ZrO_2 would contain more defects upon reduction. The shifts of Zr 3d spectra of reduced catalysts revealed that those catalysts calcined at high temperatures had more partially reduced $Zr^{\delta+}$ sites and oxygen vacancies than those calcined at low temperatures.

4.2. The structure-performance relationships

The evolutions of microstructural and surface properties greatly modulated the synergy of Cu, ZrO_2 and Al_2O_3 sites; and thus, changed the catalytic performance. The CZA-550 catalyst had the highest surface Cu sites while CZA-650 catalyst had the highest acid concentration (Fig. 9). The CZA-750 catalyst possessed only 66.0 percent of the metallic Cu sites of CZA-550 catalyst and only 77.5% of the acid sites of CZA-650 catalyst (Fig. 9). For ZrO_2 sites, only calcination at high temperatures (750, 850 °C) generated the evident crystalline ZrO_2 which has more reactivity on hydrogenation of C=O bonds [16]. However, only CZA-750 catalyst exhibited the highest ethanol yield. The data indicated that the cascade reaction of DMO-to-ethanol is not governed by a single parameter (metallic Cu sites, surface acidity or crystalline ZrO_2), rather the concurrence

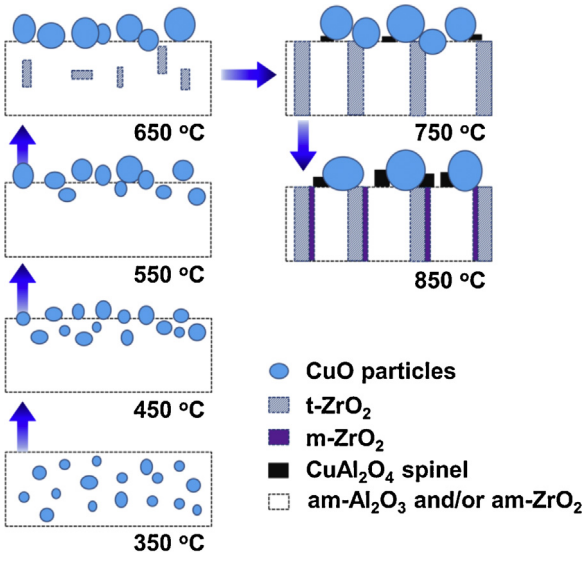

Scheme 2. Structural evolutions over the ternary CZA catalyst upon increasing calcination temperatures (am: amorphous; t: tetragonal; m: monoclinic).

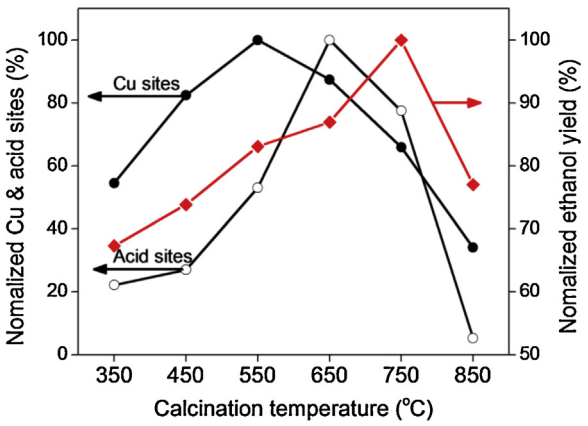

Fig. 9. The normalized Cu sites, acid sites and the normalized ethanol yield at 0.6 h^{-1} (conditions: 270 °C, 4 MPa, H_2/DMO = 150) as a function of calcination temperature (normalized: the highest is 100%).

of many factors [3,19]. This phenomenon can be explained by the synergistic effects of Cu^0–Cu^+ sites, ZrO_2 and Al_2O_3 sites.

Surface Cu^0 sites can dissociatively adsorb H_2 and facilitate the hydrogenation and/or hydrogenolysis reactions [14,48,49]. Cu^+ sites can act as electrophilic sites to polarize and activate the C=O bonds; and thus, cooperate with Cu^0 sites to improve the reactivity of catalyst. The synergistic effect between balanced Cu^0 and Cu^+ sites was well demonstrated by Fan's and Gong's groups [3,10,14,40]. Although the exposed Cu^0 sites were decreased, the high temperature calcination enhanced the strong interactions between CuO and Al_2O_3 and promoted the formation of $CuAl_2O_4$ spinel. The strong interactions and the $CuAl_2O_4$ spinel greatly retarded the reduction of Cu^{2+} species, generating more proportions of Cu^+ sites.

The ZrO_2 species over the ternary catalysts upon high temperature calcination were motivated into active tetragonal and/or monoclinic phases as evidenced by the XRD results. XPS data indicated that these ZrO_2 species would exhibited more vacancies after reduction. Crystalline ZrO_2 was reported to have promotion effects on hydrogenation of C=O bonds [16,50]. It can be partially reduced to generate some oxygen vacancies which have lower coordination numbers. The vacancies can affiliate the C=O bonds and contribute to the activation of these bonds [20,50].

The numbers of surface acid sites were also modulated by the calcination temperature. The metal–acid bifunctional can be balanced at the middle calcination temperature to catalyze the hydrogenolysis of C—O bonds efficiently [11,15,51,52]. The further calcination at 850 °C significantly promoted the sintering of catalysts and decreased both the surface Cu^0 sites and the acid sites. Thus, both the hydrogenation and hydrogenolysis abilities of catalysts were reduced at 850 °C. The CZA-750 catalyst featured with modulated Cu^0–Cu^+ sites, acid sites and crystalline ZrO_2, exhibited the best synergy effects of ternary sites and the highest ethanol yield.

Since the synergistic effects of ternary sites were tailored by the calcination temperature, the reactivity was therefore not strongly dependent on the dispersion of Cu phases. The deactivation mainly caused by Cu sintering can be conquered. Herein, an alternative way to enhance the catalyst stability for hydrogenation–hydrogenolysis reactions was provided by annealing the metal particles into stable large ones and assembling the ternary synergistic sites to compensate for the reactivity. The calcination at 750 °C facilitated the particle growth of Cu particles. These large and stable Cu particles had higher sintering temperatures. Moreover, the partially reduced Cu^+ species are indispensable sites for strengthening the metal-support interactions [40]. The enhanced metal-support interaction contributed to the immobilization of Cu particles. The enhanced metal-support interaction, together with the formation of large stable Cu particles; thus, greatly improved the catalyst stability (>200 h).

5. Conclusions

The conversion of syngas-derived dimethyl oxalate to ethanol is a cascade reaction, involving both the hydrogenation of C=O bonds and hydrogenolysis of C—O bonds. Herein, the ternary composites composed of metallic Cu, crystalline ZrO_2 and acid Al_2O_3 were constructed to catalyze the reaction efficiently for the first time. The structural evolutions and synergies of the ternary components were modulated by calcination temperature. For CuO species, elevation of calcination temperature induced surface enrichment of CuO phases, the growth of particle sizes, and the formation of $CuAl_2O_4$ spinel, which caused the change of surface Cu sites and Cu^0–Cu^+ balance. For ZrO_2 component, it transformed with the sequence of amorphous → tetragonal → monoclinic phases when the calcination temperature was increased from 350 to 850 °C. The amount of surface acid sites increased in 350–650 °C and then decreased with the further increase of calcination temperature.

We demonstrated that the cascade dimethyl oxalate to ethanol is not only determined by the metal sites, but also greatly influenced by the oxide components. The Cu–ZrO_2 synergy could promote the C=O hydrogenation while the Cu–Al_2O_3 could facilitate the hydrogenolysis of C—O bonds. Despite of the low concentration of surface metallic Cu sites, the composite calcined at 750 °C exhibited the maximum ethanol yield of 97.4% and stable performance over 200 h, which is the best reported to our knowledge. The results here provide more rational choices of high-performance catalysts for ethanol synthesis and have great implication for catalyst design for C=O hydrogenation and C—O hydrogenolysis reactions.

Acknowledgements

This work was financially supported by theMajor State Basic Research Development Program of China (973 Program) (No.2012CB215305). We would like to thank Dr. Guoqiang Ding for the helpful discussions.

Appendix A. Supplementary data

Supplementary data associated with this article can be found, in the online version, at http://dx.doi.org/10.1016/j.apcatb.2014.12.015.

References

[1] J. Goldemberg, Science 315 (2007) 808–810.
[2] H. Song, U.S. Ozkan, J. Catal. 261 (2009) 66–74.
[3] H. Yue, X. Ma, J. Gong, Acc. Chem. Res. 47 (2014) 1483–1492.
[4] J. Goldemberg, Energy Environ. Sci. 1 (2008) 523–525.
[5] P. Lv, Z. Yuan, C. Wu, L. Ma, Y. Chen, N. Tsubaki, Energy Convers. Manage. 48 (2007) 1132–1139.
[6] Y. Zhu, X. Kong, X. Li, G. Ding, Y. Zhu, Y.-W. Li, ACS Catal. 4 (2014) 3612–3620.
[7] J.J. Spivey, A. Egbebi, Chem. Soc. Rev. 36 (2007) 1514–1528.
[8] M. Gupta, M.L. Smith, J.J. Spivey, ACS Catal. 1 (2011) 641–656.
[9] S.Y. Peng, Z.N. Xu, Q.S. Chen, Y.M. Chen, J. Sun, Z.Q. Wang, M.S. Wang, G.C. Guo, Chem. Commun. 49 (2013) 5718–5720.
[10] J. Gong, H. Yue, Y. Zhao, S. Zhao, L. Zhao, J. Lv, S. Wang, X. Ma, J. Am. Chem. Soc. 134 (2012) 13922–13925.
[11] Y. Zhu, Y. Zhu, G. Ding, S. Zhu, H. Zheng, Y. Li, Appl. Catal. A: Gen. 468 (2013) 296–304.
[12] C. Mohr, H. Hofmeister, J. Radnik, P. Claus, J. Am. Chem. Soc. 125 (2003) 1905–1911.
[13] J. Zheng, H. Lin, X. Y.-n. Wang, Zheng, X. Duan, Y. Yuan, J. Catal. 297 (2013) 110–118.
[14] A. Yin, X. Guo, W. Dai, K. Fan, J. Phys. Chem. C 113 (2009) 11003–11013.
[15] S. Zhu, X. Gao, Y. Zhu, Y. Zhu, H. Zheng, Y. Li, J. Catal. 303 (2013) 70–79.

[16] Y. Zhu, X. Kong, D.-B. Cao, J. Cui, Y. Zhu, Y.-W. Li, ACS Catal. 4 (2014) 3675–3681.
[17] G. Bonura, M. Cordaro, L. Spadaro, C. Cannilla, F. Arena, F. Frusteri, Appl. Catal. B: Environ. 140–141 (2013) 16–24.
[18] G. Bonura, M. Cordaro, C. Cannilla, F. Arena, F. Frusteri, Appl. Catal. B: Environ. 152–153 (2014) 152–161.
[19] F. Frusteri, M. Cordaro, C. Cannilla, G. Bonura, Appl. Catal. B: Environ. 162 (2015) 57–65.
[20] Q.-L. Tang, Q.-J. Hong, Z.-P. Liu, J. Catal. 263 (2009) 114–122.
[21] H. Jiang, H. Bongard, W. Schmidt, F. Schüth, Micropor. Mesopor. Mater. 164 (2012) 3–8.
[22] G. Busca, Catal. Today 226 (2014) 2–13.
[23] M.V. Twigg, M.S. Spencer, Appl. Catal. A: Gen. 212 (2001) 161–174.
[24] L.-C. Wang, Q. Liu, M. Chen, Y.-M. Liu, Y. Cao, H.-Y. He, K.-N. Fan, J. Phys. Chem. C 111 (2007) 16549–16557.
[25] M.-F. Luo, P. Fang, M. He, Y.-L. Xie, J. Mol. Catal. A: Chem. 239 (2005) 243–248.
[26] S. Nishimura, T. Shishido, K. Ebitani, K. Teramura, T. Tanaka, Appl. Catal. A: Gen. 387 (2010) 185–194.
[27] A. Bienholz, R. Blume, A. Knop-Gericke, F. Girgsdies, M. Behrens, P. Claus, J. Phys. Chem. C 115 (2010) 999–1005.
[28] M. Behrens, I. Kasatkin, S. Kühl, G. Weinberg, Chem. Mater. 22 (2010) 386–397.
[29] Y.-H. Huang, S.-F. Wang, A.-P. Tsai, S. Kameoka, Ceram. Int. 40 (2014) 4541–4551.
[30] J. Irwin, T. Wei, J. Phys.: Condens. Matter 3 (1999) 299–306.
[31] J. Xu, W. Ji, Z. Shen, W. Li, S. Tang, X. Ye, D. Jia, X. Xin, J. Raman Spectrosc. 30 (1999) 413–415.
[32] Y. Kusunoki, T. Miyazawa, K. Kunimori, K. Tomishige, Catal. Commun. 6 (2005) 645–649.
[33] Y. Nakagawa, X. Ning, Y. Amada, K. Tomishige, App. Catal. A: Gen. 433–434 (2012) 128–134.
[34] J.B. Peri, R.B. Hannan, J. Phys. Chem. 64 (1960) 1526–1530.
[35] J. Peri, J. Phys. Chem. 69 (1965) 220–230.
[36] D. Lopez, K. Suwannakarn, D. Bruce, J. Goodwinjr, J. Catal. 247 (2007) 43–50.
[37] J. Gao, C. Jia, J. Li, M. Zhang, F. Gu, G. Xu, Z. Zhong, F. Su, J. Energy Chem. 22 (2013) 919–927.
[38] L. Chen, P. Guo, M. Qiao, S. Yan, H. Li, W. Shen, H. Xu, K. Fan, J. Catal. 257 (2008) 172–180.
[39] S.D. Jones, L.M. Neal, H.E. Hagelin-Weaver, Appl. Catal. B: Environ. 84 (2008) 631–642.
[40] C. Wen, Y. Cui, X. Chen, B. Zong, W.-L. Dai, Appl. Catal. B: Environ. 162 (2015) 483–493.
[41] A. Venugopal, J. Palgunadi, J.K. Deog, O.-S. Joo, C.-H. Shin, J. Mol. Catal. A: Chem. 302 (2009) 20–27.
[42] T. Ebina, T. Iwasaki, A. Chatterjee, M. Katagiri, G.D. Stucky, J. Phys. Chem. B 101 (1997) 1125–1129.
[43] R.F. Cooley, J.S. Reed, J. Am. Ceram. Soc. 55 (1972) 395–398.
[44] K.E. Sickafus, J.M. Wills, N.W. Grimes, J. Am. Ceram. Soc. 82 (1999) 3279–3292.
[45] S.-m. Chang, R.-a. Doong, Chem. Mater. 17 (2005) 4837–4844.
[46] Y. Cui, C. Wen, X. Chen, W.-L. Dai, RSC Adv. 4 (31) (2014) 162–31165.
[47] S. Zhao, H. Yue, Y. Zhao, B. Wang, Y. Geng, J. Lv, S. Wang, J. Gong, X. Ma, J. Catal. 297 (2013) 142–150.
[48] M. Behrens, F. Studt, I. Kasatkin, S. Kühl, M. Hävecker, F. Abild-Pedersen, S. Zander, F. Girgsdies, P. Kurr, B.L. Kniep, M. Tovar, R.W. Fischer, J.K. Nørskov, R. Schlögl, Science 336 (2012) 893–897.
[49] S. Natesakhawat, J.W. Lekse, J.P. Baltrus, P.R. Ohodnicki, B.H. Howard, X. Deng, C. Matranga, ACS Catal. 2 (2012) 1667–1676.
[50] B. Peng, X. Yuan, C. Zhao, J.A. Lercher, J. Am. Chem. Soc. 134 (2012) 9400–9405.
[51] I. Gandarias, P.L. Arias, J. Requies, M.B. Güemez, J.L.G. Fierro, Appl. Catal. B: Environ. 97 (2010) 248–256.
[52] S. Zhu, X. Gao, Y. Zhu, Y. Zhu, X. Xiang, C. Hu, Y. Li, Appl. Catal. B: Environ. 140–141 (2013) 60–67.